Large nitric acid particles at the top of an Arctic stratospheric cloud

Terry Deshler,[1] Niels Larsen,[2] Christoph Weissner,[3] Jochen Schreiner,[3] Konrad Mauersberger,[3] Francesco Cairo,[4] Alberto Adriani,[4,5] Guido Di Donfrancesco,[6] Joelle Ovarlez,[7] Henri Ovarlez,[7] Ulrich Blum,[8] K. H. Fricke,[8] and Andreas Dörnbrack[9]

Received 3 February 2003; revised 30 March 2003; accepted 9 April 2003; published 27 August 2003.

[1] In early December 2001, balloon-borne in situ measurements of particle composition, size, number, phase, and backscatter were completed in an Arctic stratospheric cloud composed of three distinct layers between 22 and 26 km. Below 24.5 km, liquid solution droplets of water, nitric acid, and sulfuric acid and a thin ice layer were observed. Above this layer the particles were primarily solid nitric acid trihydrate. Just above 26 km, at cloud top, where temperatures were near or above the equilibrium temperature for nitric acid trihydrate, there was a thin layer of solid particles narrowly distributed around a radius of 2.0 μm at concentrations of <0.001 cm^{-3}. Lidar backscatter and particle phase measurements approximately 200 km upwind of the in situ measurements indicate a similar vertical structure for the cloud. These in situ measurements represent, to our knowledge, the most comprehensive in situ observations of all phases of polar stratospheric cloud particles, while the large particles at cloud top have not been previously observed and may have implications for producing particles large enough to remove reactive nitrogen from the polar stratosphere. *INDEX TERMS:* 0305 Atmospheric Composition and Structure: Aerosols and particles (0345, 4801); 0320 Atmospheric Composition and Structure: Cloud physics and chemistry; 0340 Atmospheric Composition and Structure: Middle atmosphere—composition and chemistry; *KEYWORDS:* polar stratospheric clouds, in situ stratospheric cloud measurements, Arctic stratospheric clouds, polar stratospheric cloud composition, balloon-borne aerosol measurements, large polar stratospheric cloud particles

Citation: Deshler, T., et al., Large nitric acid particles at the top of an Arctic stratospheric cloud, *J. Geophys. Res.*, *108*(D16), 4517, doi:10.1029/2003JD003479, 2003.

1. Introduction

[2] Clouds in the winter polar stratosphere, leading to remarkable optical displays, have been observed for over 100 years [*Stanford and Davis*, 1974]; however, satellite observations were required to establish that gases other than water vapor were involved [*McCormick et al.*, 1982]. The role of these clouds in large spring time polar ozone loss [*Solomon et al.*, 1986; *Tolbert et al.*, 1988] has stimulated significant research activity which identified nitric acid and water as the condensable vapors [*Crutzen and Arnold*, 1986; *Toon et al.*, 1986]. The particle types which comprise these clouds include nitric acid trihydrate (NAT), a stable hydrate that can exist up to ~6 K above the ice point, T_{ICE} [*Hanson and Mauersberger*, 1988; *Voigt et al.*, 2000], liquid solution droplets of mainly water and nitric acid, which exist up to ~3 K above T_{ICE} [*Dye et al.*, 1992; *Tabazadeh et al.*, 1994; *Carslaw et al.*, 1994], and finally ice particles [*Poole and McCormick*, 1988; *Goodman et al.*, 1989]. These cloud particles form on the ubiquitous water and sulfuric acid aerosol particles pervading the stratosphere even during long volcanically quiescent periods [*Junge et al.*, 1961; *Thomason et al.*, 1997; *Deshler et al.*, 2003].

[3] Laboratory and field measurements have established that nucleation barriers exist for the formation of both NAT and ice [*Zhang et al.*, 1996; *Koop et al.*, 1997; *Carslaw et al.*, 1998]. In contrast, the liquid particles, supercooled ternary solution (STS) droplets, have no formation barrier and exist, within kinetic constraints, in thermodynamic equilibrium with their atmospheric environment [*Tabazadeh et al.*, 1994; *Carslaw et al.*, 1994; *Schreiner et al.*, 1999]. The nucleation of NAT remains a key open question which is important because of NAT's stability at relatively warm stratospheric temperatures [*Hanson and Mauersberger*, 1988], and its role in removing reactive nitrogen from the

[1]Department of Atmospheric Science, University of Wyoming, Laramie, Wyoming, USA.
[2]Danish Meteorological Institute, Copenhagen, Denmark.
[3]Bereich Atmosphärenphysik, Max-Planck-Institute für Kernphysik, Heidelberg, Germany.
[4]Institute for Atmospheric Science and Climate, Consiglio Nazionale Delle Ricerche, Rome, Italy.
[5]Now at Institute for Interplanetary Space Physics, Consiglio Nazionalle delle Ricerche, Rome, Italy.
[6]Enter per le Nuove Tecnologie, L'Energia e l'Ambiente, Centro Ricerche Energia Casaccia, Rome, Italy.
[7]Laboratoire de Meteorologie Dynamique CNRS/IPSL, Ecole Polytechnique, Palaiseau, France.
[8]Physikalisches Institut, University of Bonn, Bonn, Germany.
[9]Institut für Physik der Atmosphäre, Deutsche Zentrum für Luft- und Raumfahrt, Oberpfaffenhofen, Wessling, Germany.

0148-0227/03/2003JD003479$09.00

stratosphere [*Fahey et al.*, 1990; *Popp et al.*, 2001]. Evidence from laboratory and field data suggests that NAT formation over relatively short time periods requires an underlying solid phase, either ice [*Koop et al.*, 1997] or another hydrate [*Zhang et al.*, 1996]. Stratospheric ice nucleation requires temperatures ~3 K below T_{ICE} [*Koop et al.*, 1997; *Carslaw et al.*, 1998], while slow freezing of NAT or nitric acid dihydrate out of concentrated aqueous nitric acid solutions also requires low temperatures which are not yet well defined [*Bertram et al.*, 2000; *Salcedo et al.*, 2001]. Different processes may be involved when particles remain below T_{NAT}, the equilibrium temperature for the existence of NAT, for long time periods [*Tabazadeh et al.*, 1995; *Larsen et al.*, 1997; *Toon et al.*, 2000], and the pathways leading to the formation of stratospheric particles with radii >7 μm [*Fahey et al.*, 2001] are under investigation [*Fueglistaler et al.*, 2002, *Carslaw et al.*, 2002; *Dhaniyala et al.*, 2002]. The observations here in the late boreal fall support some of these ideas, yet they also raise new questions regarding the formation of large solid polar stratospheric cloud (PSC) particles.

2. Instrumentation and Meteorology

[4] The observations were made on 9 December 2001 from a balloon-borne gondola designed to provide detailed in situ measurements of particle composition, size, number concentration, phase, and backscatter. The thermodynamic environment was characterized with pressure, temperature, and water vapor measurements. Lidar measurements [*Müller et al.*, 1997] prior to and throughout the flight were performed at Esrange (68°N, 21°E) where the balloon was released. Particle composition was measured with an aerosol mass spectrometer [*Schreiner et al.*, 2002b] which alternated between sampling primarily masses 18 (H_2O) and 63 (HNO_3) simultaneously, and mass 46, a fragment of HNO_3 created in the ionization process. Masses 18 and 63 are sampled 43% of the time and mass 46 17% of the time. The remaining time is used for other masses and in flight calibration cycles.

[5] Particle size and number concentration were measured with four optical particle counters [*Deshler and Oltmans*, 1998; *Deshler et al.*, 2003]. One measured condensation nuclei (CN), r > 0.01 μm, and three measured particles with r > 0.15–10.0 μm. The three instruments included one with a 20 cm vertical inlet, a 20 cm horizontal inlet, and a 75 cm horizontal inlet heated to 244 K. These instruments are typically flown with a 20 cm vertical inlet. The horizontal inlet was included to provide, perhaps, a better measurement during descent; however, this was not the case. Although concentrations from the two instruments for radii <1.0 μm are similar, there are differences at larger sizes. More large particles were observed with the vertical inlet during both ascent and slow descent. Evidently few large particles make the turn into the horizontal inlet. For this reason the data presented here are from the vertical inlet instrument. The heated inlet was used to evaporate PSC particles and thus measure the background stratospheric particles upon which PSCs condense. The concentration detection limit for these instruments is 6×10^{-4} cm^{-3}.

[6] Particle phase was inferred from depolarization measurements at 532 nm using a laser backscattersonde [*Adriani et al.*, 1999]. This instrument also measured backscatter at 532 and 680 nm. In addition a second optical instrument measured backscatter at 940 and 480 nm [*Rosen and Kjome*, 1991]. Water vapor was measured with a frost point hygrometer [*Ovarlez and Ovarlez*, 1994].

[7] The temperature measurements are from Vaisala temperature sensors which have a precision of 0.1 K. Two Vaisala sensors were used and two thermistors; however, the thermistors had a precision of over 1.0 K at the coldest temperatures thus they only provided a qualitative check on the Vaisala measurements. Considering the difficulties in measuring temperature from a balloon gondola, and the correspondence of the various sensors, we estimate an accuracy of 0.5 K for the temperatures reported here.

[8] The measured temperature will be compared in this analysis with T_{NAT}, T_{STS}, and T_{ICE}. T_{NAT} is calculated from *Hanson and Mauersberger* [1988]. T_{STS} is defined as the temperature at which liquid particle volume changes by 30% for a temperature step of 0.1 K because of the condensation of nitric acid and water, and is calculated from [*Carslaw et al.*, 1995]. T_{ICE} is measured. T_{NAT} and T_{STS} are calculated using the measured water vapor and assuming 5 and 11 ppbv HNO_3. Gas phase HNO_3 was not measured during the flight, and there are no other HNO_3 measurements available during early December 2001; however, because these observations occur during the initial cold period of the winter, making denitrification unlikely, an unperturbed profile is reasonable. The range of HNO_3 used here is based on three dimensional chemical transport model profiles for the time and location of the observations (Franck Lefevre, personal communication, 2002). These values are consistent with observations in earlier winters [*Oelhaf et al.*, 1994; *Arnold et al.*, 1998].

[9] The measurements presented here captured one of the first periods of PSC formation during the 2001/2002 polar winter. The first significant cooling started in the middle of November 2001 in large amplitude gravity waves over Greenland and Scandinavia. On a synoptic scale, cold air then extended over northern Russia in a short period from 22 to 26 November; however, further cooling and deepening of the polar vortex was disrupted by a vortex splitting (minor warming) from 26 November to 2 December. One of the vortices intensified over Greenland during the following days and the air inside cooled to minimum synoptic-scale temperatures of 185 K at 30 hPa stretching from Iceland to Finland around the date of observations. Zonal flow across the Scandinavian Mountains on 9 December excited mountain waves which propagated into the stratosphere where adiabatic cooling lowered the temperature by up to 10 K compared to synoptic-scale temperatures upstream. The meteorological analysis used the mesoscale forecast model MM5, initialized by the 0000 and 1200 UT analyses of the European Center for Medium Range Weather Forecast (ECMWF). The 3 km grid spacing used is capable of resolving fine-scale lee wave activity [*Dörnbrack et al.*, 1999, 2002].

3. Arctic Stratospheric Cloud Observations

[10] A weak PSC was first observed above Esrange at 1400 (all times UT) on 9 December by lidar. This cloud grew in intensity to reach its maximum between 1900 and

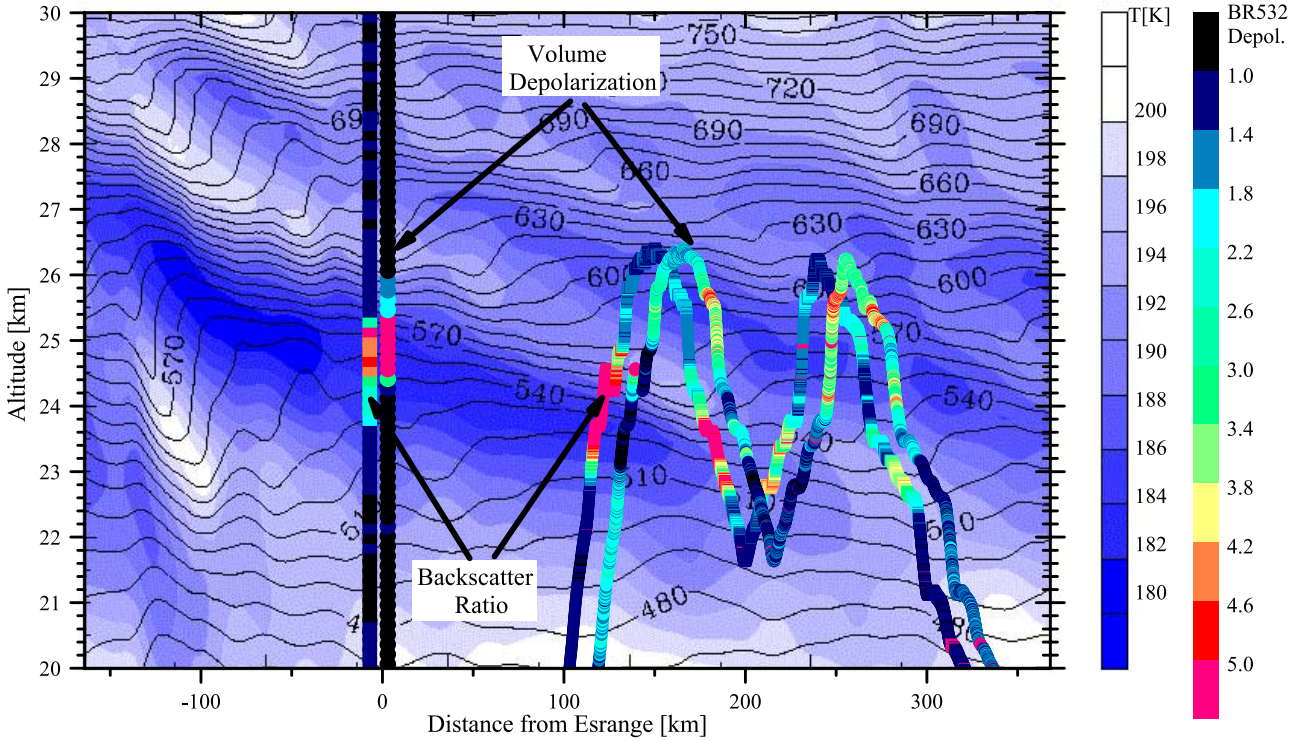

Figure 1. Height versus distance cross section, along the balloon trajectory, of temperature and potential temperature at 0000 UT on 10 December. The cross section is a 12 hour forecast from the MM5 mesoscale model using a domain of 3 km and initialized by the ECMWF model at 1200 UT on 9 December. Since there was very little directional shear the balloon trajectory could be approximated by a single MM5 cross section. Superposed on the temperature/potential temperature field is scattering ratio and volume depolarization at 532 nm measured above Esrange by lidar and along the balloon trajectory by backscattersonde on the balloon gondola. The backscatter and depolarization profiles are offset around the point of measurement. The lidar profiles were selected to capture air parcels which would advect to the in situ sampling points.

2330 at altitudes of 24–25.5 km above Esrange. Depolarization of the lidar beam indicated a region of sparse solid particles extending to approximately 26 km. The balloon-borne instruments were released at 2026 and made two ascents and descents through a PSC between 120 and 330 km downwind of Esrange, Figure 1. The PSC was observed between 22 and 26.3 km (500–620 K potential temperature) from 2145 to 0022. Above the maximum altitude of the balloon mountain wave activity diminished and did not produce enough local cooling to form clouds.

[11] The PSC sampled could be separated into three relatively distinct altitude (potential temperature) layers on the basis of the in situ measurements, Figures 1 and 2. In the lowest layer (~500–560 K potential temperature, 22.5–24.5 km) the particles were primarily STS with a thin embedded ice layer. In the middle layer (~560–600 K, 24.5–26 km) the particles were primarily NAT. Above the NAT layer, the balloon floated in a cloud top layer with a low concentration of large, solid particles containing significant amounts of water and nitric acid. The particle characteristics in these three layers were relatively well preserved on the two ascents and descents through the cloud. The three cloud layers are indicated in Figure 2.

[12] In the lower portion of the cloud, temperatures were at or below T_{STS}, volume depolarization was low, suggesting predominantly liquid droplets, particles with radii >0.15 μm increased to near CN concentrations, the concentration of 0.5–1.0 μm particles increased significantly, while the concentration of particles >1.0 μm was low. There were high water and nitric acid count rates with H_2O:HNO_3 molar ratios ranging from 3.5 ± 2 to 10 ± 3. Particle molar ratios on the second ascent and descent through the STS cloud, spanning the broad nitric acid peaks, are 3.5 ± 1, which is consistent with the coexistence of both NAT and STS. The low-volume depolarization in these regions suggests STS dominated the particle population. At the base of the first descent, 83000 s, backscattering is near background, depolarization low, and 0.15 μm particle concentrations are slightly above similar observations below the PSC (<78100 s and >87900 s); however, 0.5–1.0 μm particle concentrations are significantly elevated as are water and nitric acid count rates. In addition aerosol volumes from the unheated instrument are above those observed with the heated inlet instrument, whereas below cloud these two measurements converge (<78100 s and >87900 s), Figure 2e. Temperatures remain near T_{STS}. The molar ratio of 4 ± 1 and measured particle volumes in

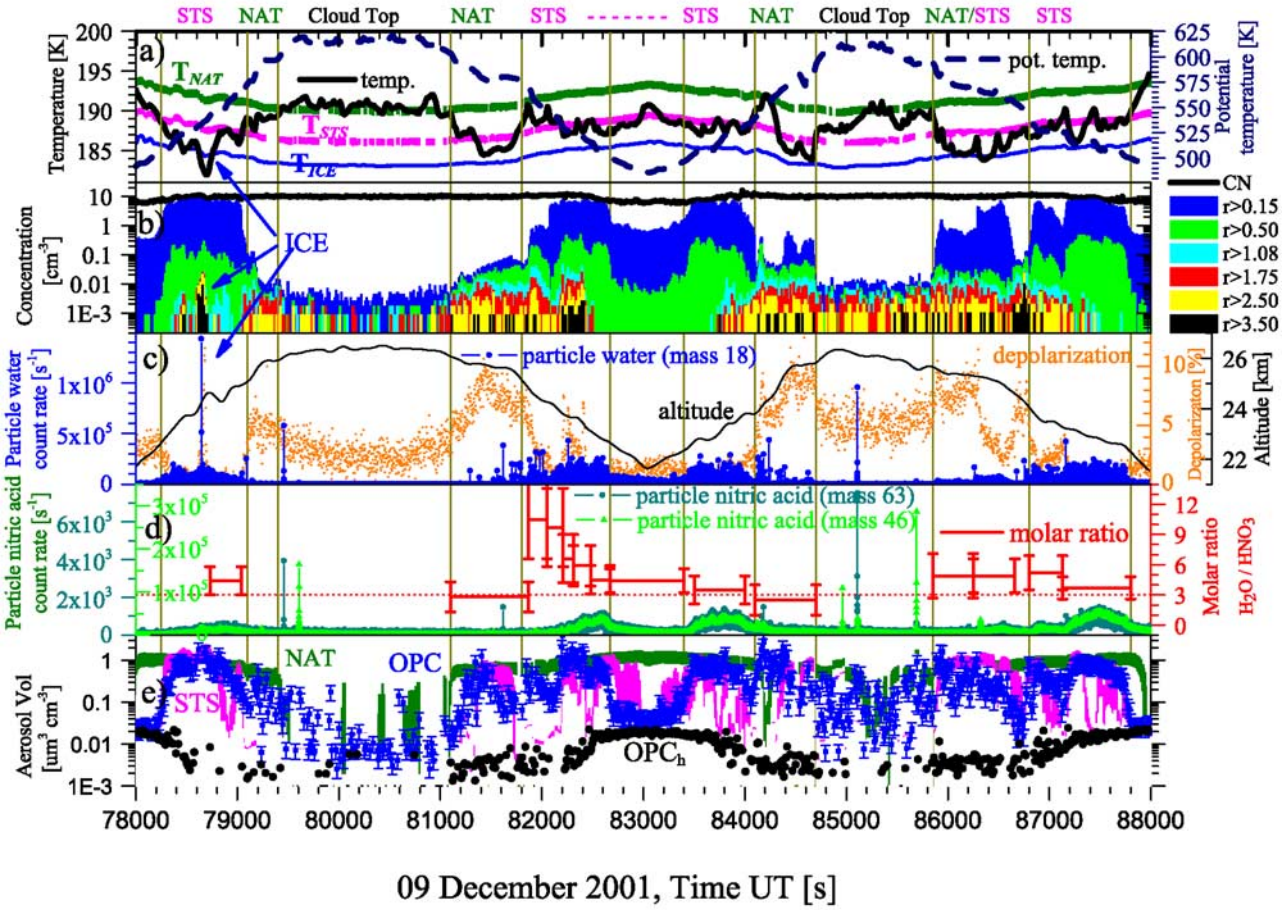

Figure 2. In situ measurements within a PSC during four transits from cloud base (potential temperature of 500 K, ~35 hPa, 22 km) to cloud top (625 K, ~15 hPa, 26.3 km). (a) Potential temperature and measured temperature compared to measured T_{ICE} and estimates of T_{NAT} and T_{STS}. The thick lines for T_{NAT} and T_{STS} indicate the range expected using the measured water and assuming 5 and 11 ppbv HNO_3. (b) Aerosol concentration at radii > 0.01 (CN), 0.15, 0.50, 1.08, 1.75, 2.50, and 3.50 μm. (c) Number of water molecules counted per second by the aerosol mass spectrometer, volume depolarization measured with the laser backscattersonde, and altitude. (d) Number of nitric acid molecules counted per second by the mass spectrometer and molar ratio. The mass 63 and mass 46 count rates are shown separately. Molar ratio for the particles sampled by the mass spectrometer are shown with error bars based on the water and nitric acid count rates. (e) Aerosol volume (μm^3 cm^{-3}) measured by the optical particle counter (OPC) with ±40% error bars, heated inlet counter (OPC_h), and theoretical aerosol volumes for NAT and STS, using the measured water and assuming 5 and 11 ppbv HNO_3, calculated using *Carslaw et al.* [1995]. The cloud regions discussed in the text are labeled at the top with separation points indicated throughout the figure.

agreement with STS model volumes suggest that the balloon remained drifting at the base of the PSC in a thin STS layer. Figure 2e shows that for the four transitions at cloud base from observations in clear air to observations in cloud the measured aerosol volume follows closely that predicted for STS [*Tabazadeh et al.*, 1994; *Carslaw et al.*, 1994] based on the measured thermodynamic properties of the air sampled and our assumptions concerning HNO_3 mixing ratios.

[13] Embedded within the STS layer on the first ascent was a narrow ice layer at 78650 s. Temperatures 3 K below T_{ICE}, and a rapid increase in depolarization, particle water mass, and particles >3.5 μm radius characterize this first comprehensive in situ observation of an ice layer within a PSC. The largest particle observed was between 5 and 10 μm radius. Backscattering in this layer, not shown, was the maximum observed throughout the flight, more than double the value of other observations in the thickest part of the PSC. The ice layer appeared as the maximum of in situ depolarization on first ascent through the cloud (Figures 1 and 2), bracketed by low depolarization in the surrounding STS layer. The mass spectrometer measured the largest water signal seen during the flight with no unusual signal in nitric acid, indicating that these ice particles formed directly from STS without incorporating additional HNO_3. On descent 55 min later through the same region of cloud, 530–540 K (82300 s), there was again an increase in depolarization and of particles >2.5 μm, including one

particle between 5 and 10 μm; however, temperatures were warmer, near T_{STS}, and no ice was observed. This layer is also observed on the second ascent and descent at ~540 K, the boundary of the NAT/STS layers, as an increase in depolarization and large particles. Consistently the largest particles observed throughout the flight correspond to this layer suggesting that the ice layer stimulated the development of large solid particles which then grew within the lower STS layer.

[14] Directly above the STS layer volume depolarization was elevated and there was a significant increase in particles ≥1.0 μm. Temperatures were both above and below T_{STS}, but always below T_{NAT}. Water and nitric acid count rates were low, but the impacts of many single particles, observed by the mass spectrometer as many single spikes, are evident, particularly on the first descent (81,100–81,800 s) and second ascent (84,100–84,700 s) through the NAT layer. Molar ratios are 3 ± 1 and 2.5 ± 1.5 on the first descent and second ascent and 5 ± 1.5 on the second descent. Composition measurements are not available on the first ascent through the NAT region because of the relatively large amount of HNO_3 accumulated in the evaporation sphere of the mass spectrometer from the lower STS layer, and the slow release of HNO_3 from the sphere. This characteristic of the mass spectrometer is unique to its initial exposure to HNO_3. Except for the final descent, all observations, particle phase, molar ratio, aerosol volume, and size, suggest the particles to be predominantly NAT in this upper layer of the PSC. On final descent the observations suggest a mixed cloud containing both STS and NAT. NAT is suggested by the presence of large particles and elevated depolarization, STS by a molar ratio of 5 and a concentration of 0.15 μm particles a factor of 10 higher than the first three encounters with the upper NAT layer. Temperatures in this layer on final descent are somewhat colder than the first three passes through the upper NAT layer, thus some STS development would be expected.

[15] The balloon-borne gondola reached its ceiling at a potential temperature of 620 K (26.5 km) and floated at this altitude for 30 min after the first ascent and 17 min after the second, Figure 2. Temperatures were at or above T_{NAT}, backscatter was low but above background, depolarization was elevated although below measurements in the NAT layers, 0.15 μm particle concentrations were <0.01 cm^{-3}, as would be expected for sulfate aerosol at these altitudes, while the concentration of particles >1.0 μm was elevated, creating a very distinct and narrow particle mode at these larger sizes, and no intervening smaller particles. Aerosol volume has large variations, but is generally above that expected for NAT, particularly for the highest measurements on the first encounter with cloud top. The low concentration of particles leads to water and nitric acid count rates below those required for determining composition. Typically a signal from PSC particles about a factor of 2 above the background sulfate aerosols is required to determine molar ratios. However, interspersed within this region of low particle concentration, five large particles were sampled. The capture of these five particles can be seen in the HNO_3 count rate on mass 63 (2 particles) and 46 (3 particles), Figure 2d. Each particle produces an HNO_3 signal above every other particle measured throughout the flight. Considering the sampling efficiency of the aerosol mass spectrometer, the estimated concentration of these particles agrees with the measured concentration from the particle counters, the derived radii lie between 1 and 1.5 μm. Unfortunately only two of the five particles were captured while H_2O (mass 18) and HNO_3 (mass 63) were being sampled simultaneously. Therefore the molar ratios can only be estimated to lie in the range between 2 and 3.

[16] The aerosol mass spectrometer provides H_2O/HNO_3 molar ratios with reasonably good accuracy when the net signals for H_2O and HNO_3 are integrated over time periods of 100 or more seconds. For the flight here, sampling frequency of selected mass peaks was increased, increasing the resolution to 100 ms. Because of this, the detection of single particles greater than >1 μm can be observed when the aerosol volume is low, as at cloud top. While these large particles can be well identified (Figures 2c and 2d), it is impossible to derive molar ratios of similar accuracy to those determined from longer integrations. Attempts were made to reconstruct the missing water peaks for the three particles that were sampled on mass 46. The results, however, were ambiguous. There are not enough constraints on the shape and amplitude of the missing water signal. While only five large particles were captured, the HNO_3 signals observed from all five particles are well above the HNO_3 signal from particles observed in all other regions of the cloud. This, coupled with the simultaneous water and nitric acid measurements on two particles, suggests that the molar ratio of these particles may be less than is expected for NAT.

[17] Evaporating NAT particles are not anticipated to produce particles with molar ratios below 3. During evaporation deviations from a NAT composition is expected only on a surface monolayer and would not significantly influence the overall molar ratio of a large NAT particle. The observations also do not support particles falling from above. At Esrange PSCs never extended above 26 km during the measurement period, and temperatures above the balloon trajectory were too warm for PSCs according to the meteorological analysis. Although NAT, or evaporating NAT, could be expected in the cloud top layer, the suggestion of even higher HNO_3 content in particles is most unusual. *Schreiner et al.* [2002a] observed a region of HNO_3 rich particles in a lee wave PSC in January 2000; however, this was in a region with smaller particles and higher concentrations at the bottom of a PSC. The observations reported here, of high HNO_3 content solid particles narrowly distributed around a radius of 2.0 μm at concentrations of less than 0.001 cm^{-3}, are unique.

4. Discussion and Conclusions

[18] Derived molar ratios and aerosol volumes are in good agreement with modeled STS ratios and volumes. Figure 3 compares, as a function of temperature, measurement and theory for these quantities for the NAT, STS, and NAT/STS mixed layers measured on 9 December 2001. In general the measured NAT volumes are more in agreement with an assumption of 5 ppbv nitric acid, whereas the STS volumes are more in agreement with an assumption of 11 ppbv. The mixed layer shows some agreement with both assumptions and is in a temperature range (<188 K) where the two model volumes overlap significantly. Both the NAT

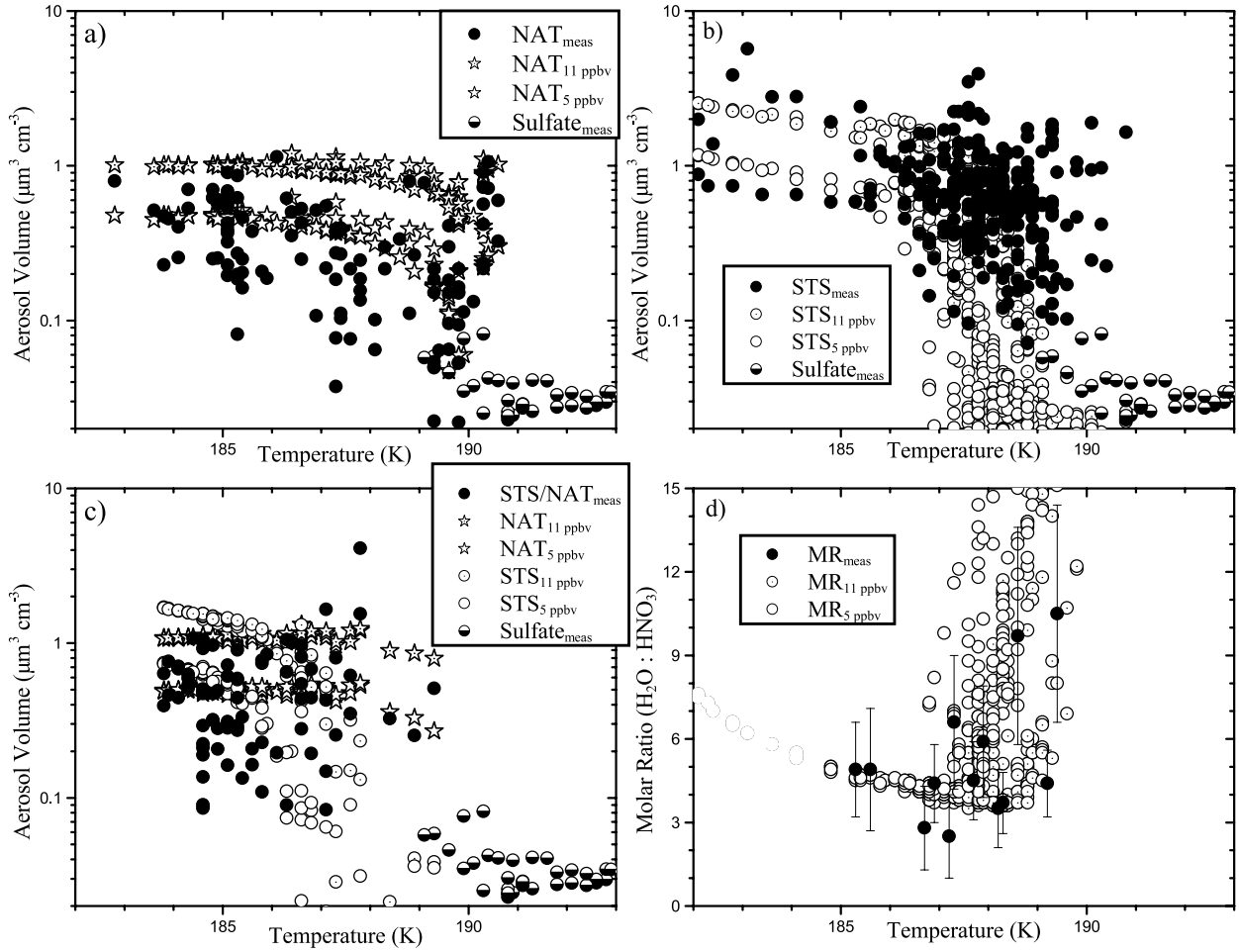

Figure 3. Comparisons, as a function of temperature, between measured and theoretical aerosol volume concentrations for (a) NAT, (b) STS, and (c) STS/NAT mixed layers and (d) molar ratios (MR) for the STS layers, all measured on 9 December 2001. For each panel, two calculations are included. They use *Carslaw et al.* [1995] and the measured water vapor mixing ratio and assume 5 and 11 ppbv nitric acid. The measurements are indicated by solid symbols and have an uncertainty of ±40%, which, for clarity, is not shown. The calculations use open symbols with the subscripts on NAT, STS, and MR indicating the nitric acid mixing ratios assumed. The sulfate aerosol volumes are from measurements beneath the PSC. The two measured molar ratios of 3 are for the NAT layers (see Figure 2) and are not expected to agree with the molar ratio calculations for STS.

and NAT/STS layers also show aerosol volumes below the theoretical calculations; whereas the STS layer does not. The measured molar ratios for both STS and NAT are compared to calculations for all of the STS layers in Figure 3d. The calculations demonstrate that molar ratios are higher when HNO_3 mixing ratios are low since less HNO_3 is available to be incorporated into the particle. The STS measurements are again more in agreement with an assumption of 11 ppbv HNO_3. The higher mixing ratio is expected on the basis of the early period of the observations prior to any denitrification. Both the volume and molar ratio calculations suggest the measured STS particles are in equilibrium with their environment whereas the NAT particles may not be.

[19] The distinct yet relatively homogeneous PSC layers observed on 9 December allow characteristic lognormal size distributions to be constructed for STS, NAT, ice, and the cloud top particles, Figure 4. NAT, ice, and the large cloud top particles all exhibit a well-defined second mode, $N_2 \sim 0.01$ cm^{-3} for NAT and ice, and $N_2 < 0.001$ cm^{-3} for the cloud top particles. For NAT and the cloud top particles the first mode median radii, ~0.01 μm, do not differ significantly from the sulfate aerosol present throughout the lower stratosphere and upon which PSC particles condense. This sulfate distribution was measured with the horizontal heated inlet instrument and is shown in Figure 4 to be comparable to the first mode of the NAT and cloud top distributions. In contrast STS layers all exhibit a first mode with a width and median radius larger than the sulfate distribution, but a poorly defined, or nonexistent, second mode. The first mode of the ice cloud is similar to the STS cloud, as expected, since the ice layer formed in the midst of an STS cloud. The difference between the stratospheric sulfate distribution and the first modes of the STS cloud and ice layer is clear in

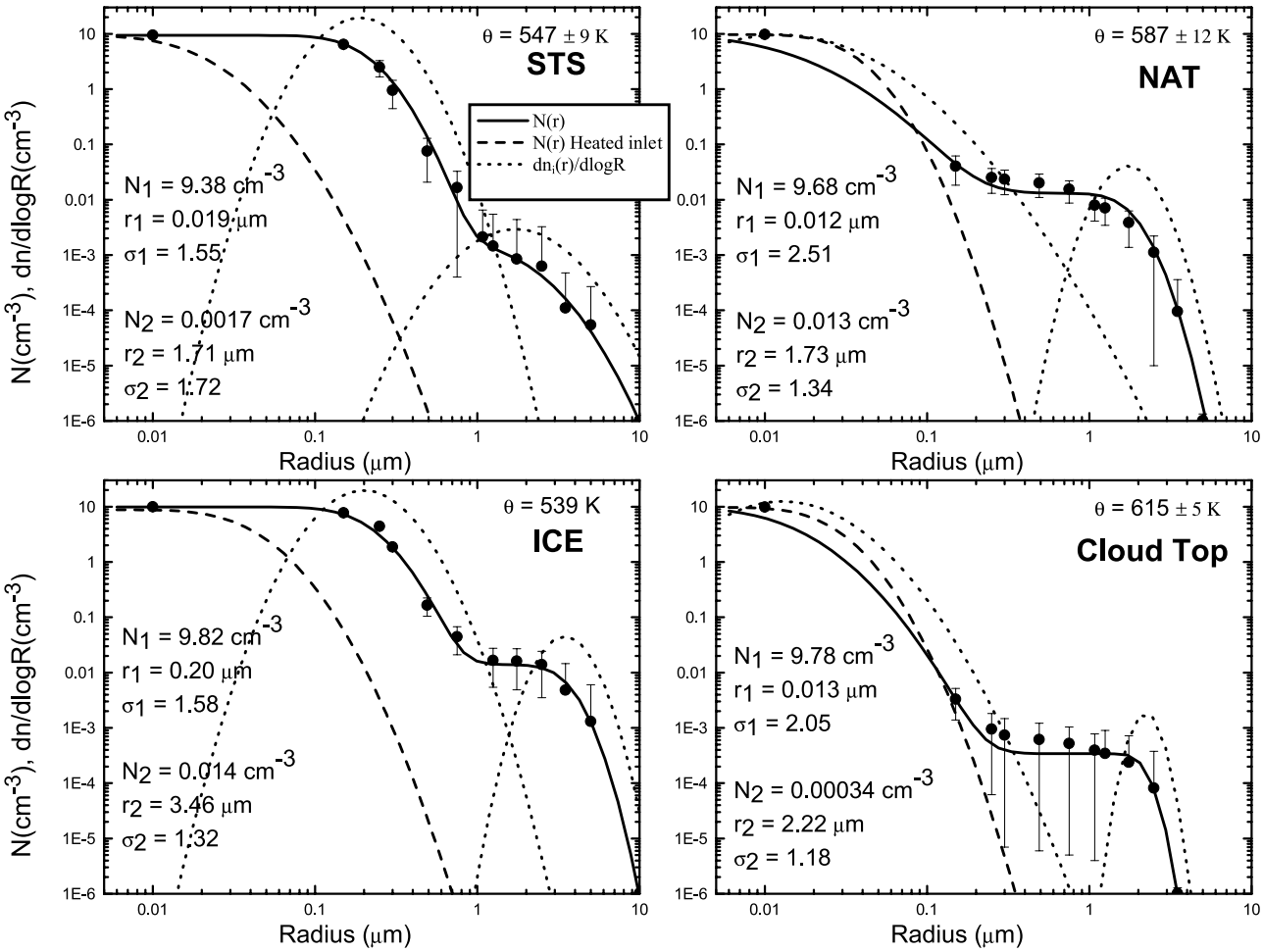

Figure 4. Bimodal lognormal size distributions fit to optical particle counter measurements (data points) within an STS, NAT, and ice layer and for observations at cloud top. In each case the observations result from averaging measurements within the various cloud layers. Error bars represent the population standard deviation of the averaged measurements and exceed measurement precision for a single measurement. Half error bars are used when the lower half of the error bar extends to the abscissa. Differential lognormal distributions for each mode of the size distribution are the dotted lines. The cumulative concentration, solid line, is what is measured by the instruments. Parameters of the size distributions are shown. The lognormal size distributions are chosen by minimizing the root mean square error = $\Sigma_i \log^2 [N_m(>r_i)/N(>r_i)]$. The summation is over all measured sizes, r_i, $N_m(>r_i)$ is the measured concentration of all particles with $r > r_i$, and $N(>r_i)$ is the sum of the bimodal lognormal size distributions. The method consists of trying all combinations of measured concentrations to find the set of five discrete sizes plus CN, giving size distribution parameters that minimize the root mean square error when all measurements are included [*Deshler et al.*, 2003]. The stratospheric sulfate distribution, measured by the heated inlet particle counter at the time of the respective PSC measurements, is shown for comparison.

Figure 4. The second modes of the ice and cloud top particles are both very narrow, peaking at 3.5 μm (ice) and 2.2 μm (cloud top), whereas the second mode of the NAT layer is broader and peaked at smaller sizes, 1.7 μm. These well-developed second modes for NAT, ice, and the cloud top particles suggest a nucleation barrier to particle formation, with larger particles, $r > 0.15$ μm, preferentially nucleated, as expected from classical nucleation theory [*Volmer and Weber*, 1926; *Frenkel*, 1955]. In contrast the broad and well developed first mode for the STS layers suggests no formation barrier, but rather condensation of H_2O and HNO_3 on all particles. In several of the STS layers the concentration of particles ≥0.15 μm nearly matches the CN concentration, as has been observed in other Arctic stratospheric clouds [*Hofmann et al.*, 1990; *Deshler and Oltmans*, 1998; *Deshler et al.*, 2000]. Condensation on many particles allows the particles to remain close to thermodynamic equilibrium.

[20] Air parcel temperature histories, estimated from back-trajectory calculations, were used to model the growth of particles within the NAT layer and at cloud top. Particles in the lower STS layer are explained with a thermodynamic

model in which the particles swell with water and nitric acid as temperatures decrease [*Tabazadeh et al.*, 1994; *Carslaw et al.*, 1994], Figures 2e and 3. Air parcel back-trajectories from the base of the NAT layer, 575 K, indicate that temperatures fluctuated from ~6 K above T_{NAT} to more than 3 K below T_{ICE} four hours prior to sampling. The temperature then rose slightly above T_{NAT} before decreasing to 2 K below T_{NAT} at the sampling point. The microphysical model applied [*Larsen et al.*, 2002] nucleates the large particle tail of the size distribution at temperatures ~3 K below T_{ICE}, when ice freezes out of STS, and in this case predicts that all particles >0.1 μm grow to particles >1.0 μm. Temperatures above T_{NAT} do not persist long enough to evaporate these particles, and the size distribution remains strongly bimodal with the large particles remaining as NAT at the sampling points, representing the dominant particle volume.

[21] At cloud top, 605 K, temperatures in the previous 8 hours remain between T_{NAT} and T_{ICE}. This minimum temperature is not sufficient to nucleate ice and NAT in this model, and the model predicts only the growth of STS between 1600 and 1800. After 1800 the temperature is above T_{STS} and all model PSC particles evaporate by the time this air parcel is sampled at 2200. This disagrees with the observations which suggest that a significant fraction of particles >0.15 μm had nucleated and grown to sizes >1 μm. These relatively large particles are expected to have originated near the layer of observation. Assuming nucleation of these particles as NAT, growth times range from 5–10 hours, depending on supersaturation with respect to HNO_3. At fall speeds for 1–3 μm particles this leads to vertical displacements of less than 50–150 m over the growth time.

[22] Because of the strong mountain wave activity on this day air parcels above approximately 23 km, 540 K, experienced large heating and cooling rates, exceeding 75 K d^{-1} just a few hours upwind of the observations. Such large heating/cooling rates can drive liquid particle compositions far out of equilibrium because of kinetic constraints, substantially increasing the HNO_3 weight fraction among the small STS particles [*Meilinger et al.*, 1995]. In these cases alternate nucleation scenarios [*Tsias et al.*, 1997] may nucleate the particles with high HNO_3 concentrations, albeit with very low nucleation rates as estimated from laboratory experiments [*Bertram et al.*, 2000; *Salcedo et al.*, 2001]. The microphysical model tested does not consider the surface nucleation of NAT [*Tabazadeh et al.*, 2002]. This nucleation path will be considered in a future analysis of these and other observations.

[23] The formation and stability of Arctic stratospheric clouds have serious implications for chlorine activation and subsequent Arctic ozone loss [*Gao et al.*, 2001]. The formation of large solid particles within these clouds controls the removal of nitrogen oxides from the stratosphere, thus impacting ozone recovery. Stratospheric temperatures, which ultimately control cloud formation, are subject to large variations in the Arctic compared to the Antarctic where the polar vortex, and hence temperatures, are more stable and colder. For both hemispheres the nucleation of solid PSC particles is a key issue; however, it is more critical in the Arctic since temperatures are often at or near T_{NAT} but seldom fall low enough for NAT nucleation from ice. In situ observations of an Arctic stratospheric cloud on 9 December 2001 capture a cloud composed of a lower liquid STS layer with an embedded ice layer, a NAT upper layer, and a cloud top with a few solid ~2.0 μm radius particles with molar ratios of 3 (consistent with NAT) or below. This picture of an STS cloud capped by a NAT cloud is consistent with the cross polarized observations of the lidar at Esrange from 1930–0000, indicating solid particles predominantly at cloud top, 25–26 km.

[24] The formation of particles within the two lower layers of this PSC fit well with models for the formation of STS, NAT, and embedded ice. This seems to be the case even though back-trajectories indicate the air parcels sampled were exposed to very large heating and cooling rates which would provide particle environments significantly out of equilibrium with their gas phase environments. The large solid particles at cloud top, however, are difficult to explain. Temperatures are too warm for STS and are at or above T_{NAT}. Temperatures upstream of the observations remain above the ice point, the nominal NAT nucleation point. The cloud top and NAT observations do suggest that the PSC particles which grew to large solid particles formed on the large particle tail of the background sulfate size distribution. These PSC observations on 9 December both substantiate present PSC particle growth and nucleation models and raise the possibility for testing alternate pathways for the formation of large solid PSC particles. Such particles may play an important role in the development and sedimentation of much larger solid HNO_3-bearing particles [*Fahey et al.*, 2001] which can cause significant denitrification of the Arctic stratosphere.

[25] **Acknowledgments.** The excellent balloon operations were completed by the Centre National d'Etudes Spatiales with support from the Swedish Space Corporation. This research was supported by the Commission of the European Union through the Energy, Environment and Sustainable Development program and the U.S. National Science Foundation.

References

Adriani, A., F. Cairo, M. Viterbini, S. Mandolini, L. Pulvirenti, and G. Di Donfrancesco, Multiwavelength aerosol scatterometer for airborne experiments to study the optical properties of stratospheric aerosol, *J. Atmos. Oceanic Technol.*, *16*, 1329–1336, 1999.

Arnold, F., V. Bürger, K. Gólinger, M. Roncossek, J. Schneider, and S. Spreng, Observations of nitric acid perturbations in the winter Arctic stratosphere: Evidence for PSC sedimentation, *J. Atmos. Chem.*, *30*, 49–59, 1998.

Bertram, A. K., D. B. Dickens, and J. J. Sloan, Supercooling of type 1 polar stratospheric clouds: The freezing of submicron nitric acid aerosols having HNO_3 mol fractions less than 0. 5, *J. Geophys. Res.*, *105*, 9283–9290, 2000.

Carslaw, K. S., B. P. Luo, S. L. Clegg, T. Peter, P. Brimblecombe, and P. J. Crutzen, Stratospheric aerosol growth and HNO_3 and water uptake by liquid particles, *Geophys. Res. Lett.*, *21*, 2479–2482, 1994.

Carslaw, K. S., B. Luo, and T. Peter, An analytic expression for the composition of aqueous HNO_3-H_2SO_4 stratospheric aerosols including gas phase removal of HNO_3, *Geophys. Res. Lett.*, *22*, 1877–1880, 1995.

Carslaw, K. S., M. Wirth, A. Tsias, B. P. Luo, A. Dörnbrack, M. Leutbecher, H. volkert, W. Renger, J. T. Bacmeister, and T. Peter, Particle microphysics and chemistry in remotely observed mountain polar stratospheric clouds, *J. Geophys. Res.*, *103*, 5785–5796, 1998.

Carslaw, K. S., J. A. Kettleborough, M. J. Northway, S. Davies, R.-S. Gao, D. W. Fahey, D. G. Baumgardner, M. P. Chipperfield, and A. Kleinböhl, A vortex-scale simulation of the growth and sedimentation of large nitric acid hydrate particles, *J. Geophys. Res.*, *107*(D20), 8300, doi:10.1029/2001JD000467, 2002.

Crutzen, P. J., and F. Arnold, Nitric acid cloud formation in the cold Antarctic stratosphere: A major cause for the springtime ozone hole, *Nature*, *324*, 651–654, 1986.

Deshler, T., and S. J. Oltmans, Vertical profiles of volcanic aerosol and polar stratospheric clouds above Kiruna, Sweden: Winters 1993 and 1995, *J. Atmos. Chem*, *30*, 11–23, 1998.

Deshler, T., B. Nardi, A. Adriani, F. Cairo, G. Hansen, F. Fierli, A. Hauchercorne, and L. Pulvirenti, Determining the index of refraction of polar stratospheric clouds above Andoya (69°N) by combining size-resolved concentration and optical scattering measurements, *J. Geophys. Res.*, *105*, 3943–3953, 2000.

Deshler, T., M. E. Hervig, D. J. Hofmann, J. M. Rosen, and J. B. Liley, Thirty years of in situ stratospheric aerosol size distribution measurements from Laramie, Wyoming (41°N), using balloonborne instruments, *J. Geophys. Res.*, *108*(D5), 4167, doi:10.1029/2002JD002514, 2003.

Dhaniyala, S., K. A. McKinney, and P. O. Wennberg, Lee-wave clouds and denitrification of the polar stratosphere, *Geophys. Res. Lett*, *29*(9), 1322, doi:10.1029/2001GL013900, 2002.

Dörnbrack, A., M. Leutbecher, R. Kivi, and E. Kyrö, Mountain wave induced record low stratospheric temperatures above Northern Scandinavia, *Tellus, Ser.A.*, *51*, 951–963, 1999.

Dörnbrack, A., T. Birner, A. Fix, A. Meister, H. Flentje, H. Schmid, E. V. Browell, and M. J. Mahoney, Evidence for inertia gravity waves forming polar stratospheric clouds over Scandinavia, *J. Geophys. Res.*, *107*(D20), 8287, doi:10.1029/2001JD000452, 2002.

Dye, J. E., D. Baumgardner, B. W. Gandrud, S. R. Kawa, K. K. Kelly, M. Loewenstein, G. V. Ferry, K. R. Chan, and B. L. Gary, Particle size distribution in Arctic polar stratospheric clouds, growth and freezing of sulfuric acid droplets, and implications for cloud formation, *J. Geophys. Res.*, *97*, 8015–8034, 1992.

Fahey, D. W., K. K. Kelly, S. R. Kawa, A. F. Tuck, M. Loewenstein, K. R. Chan, and L. E. Heidt, Observation of denitrification and dehydration in the winter polar stratospheres, *Nature*, *344*, 321–324, 1990.

Fahey, D. W., et al., The detection of large HNO_3-containing particles in the winter Arctic stratosphere, *Science*, *291*, 1026–1031, 2001.

Frenkel, J., *Kinetic Theory of Liquids*, Dover, Mineola, N.Y., 1955.

Fueglistaler, S., et al., Large NAT particle formation by mother clouds: Analysis of SOLVE/THESEO-2000 observations, *Geophys. Res. Lett*, *29*(12), 1610, doi:10.1029/2001GL014548, 2002.

Gao, R. S., et al., Observational evidence for the role of denitrification in Arctic stratospheric ozone loss, *Geophys. Res. Lett.*, *28*, 2879–2882, 2001.

Goodman, J., O. B. Toon, R. F. Pueschel, K. G. Snetsinger, and S. Verma, Antarctic stratospheric ice clouds, *J. Geophys. Res.*, *94*, 16,449–16,458, 1989.

Hanson, D. R., and K. Mauersberger, Laboratory studies of the nitric acid trihydrate: Implication for the south polar stratosphere, *Geophys. Res. Lett.*, *15*, 855–858, 1988.

Hofmann, D. J., T. Deshler, F. Arnold, and H. Schlager, Balloon observations of nitric acid aerosol formation in the arctic stratosphere: II. Aerosol, *Geophys. Res. Lett*, *17*, 1279–1282, 1990.

Junge, C. E., C. W. Changnon, and J. E. Manson, Stratospheric aerosols, *J. Meteorol*, *18*, 81–108, 1961.

Koop, T., B. P. Luo, U. M. Biermann, P. J. Crutzen, and T. Peter, Freezing of $HNO_3/H_2SO_4/H_2O$ solutions at stratospheric temperatures: Nucleation statistics and experiments, *J. Phys. Chem. A*, *101*, 1117–1133, 1997.

Larsen, N., B. M. Knudsen, J. M. Rosen, N. T. Kjome, R. Neuber, and E. Kyrö, Temperature histories in liquid and solid polar stratospheric cloud formation, *J. Geophys. Res.*, *102*, 23,505–23,517, 1997.

Larsen, N., et al., Microphysical mesoscale simulations of polar stratospheric cloud formation constrained by in situ measurements of chemical and optical cloud properties, *J. Geophys. Res.*, *107*(D20), 8301, doi:10.1029/2001JD000999, 2002.

McCormick, M. P., H. M. Steele, P. Hamill, W. P. Chu, and T. J. Swissler, Polar stratospheric cloud sightings by SAM II, *J. Atmos. Sci.*, *39*, 1387–1397, 1982.

Meilinger, S. K., T. Koop, B. P. Luo, T. Huthwelker, K. S. Carslaw, U. Krieger, P. J. Crutzen, and T. Peter, Size-dependent stratospheric droplet composition in lee wave temperature fluctuations and their potential role in PSC freezing, *Geophys. Res. Lett.*, *22*, 3031–3034, 1995.

Müller, K., G. Baumgarten, J. Siebert, and K. H. Fricke, The new lidar facility at Esrange, Kiruna, paper presented at 13th ESA Symposium on European Rocket and Balloon Programmes and Related Research, Eur. Space Agency, Öland, Sweden, 1997.

Oelhaf, H., T. v. Clarmann, H. Fischer, F. Freidl-Vallon, Ch. Fritzsche, A. Linden, Ch. Piesch, M. Seefeldner, and W. Völker, Stratospheric $CLONO_2$ and HNO_3 profiles inside the Arctic vortex from MIPSA-B limb emission spectra obtained during EASOE, *Gephys. Res. Lett.*, *21*, 1263–1266, 1994.

Ovarlez, J., and H. Ovarlez, Stratospheric water vapor content evolution during EASOE, *Geophys. Res. Lett.*, *21*, 1235–1238, 1994.

Poole, L. R., and M. P. McCormick, Airborne lidar observations of Arctic polar stratospheric clouds: Indications of two distinct growth stages, *Geophys. Res. Lett.*, *15*, 21–23, 1988.

Popp, P. J., et al., Severe and extensive denitrification in the 1999–2000 Arctic winter stratosphere, *Geophys. Res. Lett.*, *28*, 2875–2878, 2001.

Rosen, J. M., and N. T. Kjome, Backscattersonde: A new instrument for atmospheric aerosol research, *J. Appl. Opt.*, *30*, 1552–1561, 1991.

Salcedo, D., L. T. Molina, and M. J. Molina, Homogeneous freezing of concentrated aqueous nitric acid solutions at polar stratospheric temperatures, *J. Phys. Chem. A.*, *105*, 1433–1439, 2001.

Schreiner, J., C. Voigt, A. Kohlmann, F. Arnold, K. Mauersberger, and N. Larsen, Chemical analysis of polar stratospheric cloud particles, *Science*, *283*, 968–970, 1999.

Schreiner, J., et al., Chemical, microphysical, and optical properties of polar stratospheric clouds, *J. Geophys. Res.*, *107*, 8313, doi:10.1029/2001JD000825, 2002a.

Schreiner, J., C. Voigt, P. Zink, A. Kohlmann, D. Knopf, C. Weisser, P. Budz, and K. Mauersberger, A mass spectrometer system for analysis of polar stratospheric aerosols, *Rev. Sci Inst.*, *73*, 446–452, 2002b.

Solomon, S., R. R. Garcia, F. S. Rowland, and D. J. Wuebbles, On the depletion of Antarctic ozone, *Nature*, *321*, 755–758, 1986.

Stanford, J. L., and J. S. Davis, A century of stratospheric cloud reports: 1870–1972, *Bull. Am. Meteorol. Soc.*, *55*, 213–219, 1974.

Tabazadeh, A., R. P. Turco, K. Drdla, and M. Z. Jacobson, A study of type I polar stratospheric cloud formation, *Geophys. Res. Lett.*, *21*, 1619–1622, 1994.

Tabazadeh, A., O. B. Toon, and P. Hamill, Freezing behavior of stratospheric sulfate aerosols inferred from trajectory studies, *Geophys. Res. Lett.*, *22*, 1725–1728, 1995.

Tabazadeh, A., Y. S. Dijikaev, P. Hamill, and H. Reiss, Laboratory evidence for surface nucleation of solid polar stratospheric cloud particles, *J. Phys. Chem. A*, *106*, 10,238–10,246, 2002.

Thomason, L. W., L. R. Poole, and T. Deshler, A global climatology of stratospheric aerosol surface area density deduced from stratospheric aerosol and gas experiment II measurements: 1984–1994, *J. Geophys. Res.*, *102*, 8967–8976, 1997.

Tolbert, M. A., M. J. Rossi, and D. M. Golden, Heterogeneous interactions of chlorine nitrate hydrogen chloride and nitric acid with sulfuric acid surfaces at stratospheric temperatures, *Geophys. Res. Lett.*, *15*, 847–850, 1988.

Toon, O. B., P. Hamill, R. P. Turco, and J. Pinto, Condensation of HNO_3 and HCl in the winter polar stratospheres, *Geophys. Res. Lett.*, *13*, 1284–1287, 1986.

Toon, O. B., A. Tabazadeh, E. V. Browell, and J. Jordan, Analysis of lidar observations of Arctic polar stratospheric clouds during January 1989, *J. Geophys. Res*, *105*, 20,589–20,615, 2000.

Tsias, A., A. J. Prenni, K. S. Carslaw, T. P. Onasch, B. P. Luo, M. A. Tolbert, and T. Peter, Freezing of polar stratospheric clouds in orographically induced strong warming events, *Geophys. Res. Lett.*, *24*, 2303–2306, 1997.

Voigt, C., et al., Nitric acid trihydrate (NAT) in polar stratospheric cloud particles, *Science*, *290*, 1756–1758, 2000.

Volmer, M., and A. Weber, Keimbildung in übersättigten gebiulden, *Z. Phys. Chem.*, *119*, 277–301, 1926.

Zhang, R., M.-T. Leu, and M. J. Molina, Formation of polar stratospheric clouds on preactivated background aerosols, *Geophys. Res. Lett.*, *23*, 1669–1672, 1996.

A. Adriani, Institute for Interplanetary Space Physics, Consiglio Nazionalle delle Ricerche, Via Fosso del Cavaliere 100, 00133 Roma, Italy.

U. Blum and K. H. Fricke, Physikalisches Institut, University of Bonn, Nussallee 12, D-53115 Bonn, Germany.

F. Cairo, Institute for Atmospheric Science and Climate, Consiglio Nazionale Delle Ricerche, Via Fosso del Cavaliere 100, 00133 Roma, Italy.

T. Deshler, Department of Atmospheric Science, University of Wyoming, Laramie, WY 82071, USA. (Deshler@uwyo.edu)

G. Di Donfrancesco, Ente per le Nuove Tecnologie, L'Energia e l'Ambiente, Centro Ricerche Energia Casaccia, 0600 S. Maria di Galeria, 00196 Roma, Italy.

A. Dörnbrack, Institut für Physik der Atmosphäre, Deutsches Zentrum für Luft- und Raumfahrt, D-82230 Oberpfaffenhofen, Germany.

N. Larsen, Danish Meteorological Institute, Lyngbyvej 100, DK-2100 Copenhagen, Denmark.

K. Mauersberger, J. Schreiner, and C. Weisser, Bereich Atmosphärenphysik, Max-Planck-Institut, für Kernphysik, Postfach 103 980, D-69029 Heidelberg, Germany.

H. Ovarlez and J. Ovarlez, Laboratoire de Meteorologie Dynamique CNRS/IPSL, Ecole Polytechnique, 91128 Palaiseau, France.